

apes and provides evidence of a link between African and Eurasian hominoids in the Middle Miocene (34).

References and Notes

1. D. Pilbeam, *Mol. Phylogenet. Evol.* **5**, 155 (1996).
2. S. C. Ward and D. R. Pilbeam, in *New Interpretations of Ape and Human Ancestry*, R. L. Ciochon and R. S. Corrucini, Eds. (Plenum, New York, 1983), pp. 325–351.
3. L. Martin, in *Major Topics in Primate and Human Evolution*, B. Wood, L. Martin, P. Andrews, Eds. (Cambridge Univ. Press, Cambridge, 1986), pp. 151–187.
4. P. Andrews and L. B. Martin, *J. Hum. Evol.* **16**, 101 (1987).
5. M. L. McCrossin and B. R. Benefit, in *Integrated Paths to the Past: Paleoanthropological Advances in Honor of F. C. Howell*, R. S. Corrucini and R. L. Ciochon, Eds. (Prentice-Hall, New York, 1994), pp. 95–122.
6. M. L. McCrossin and B. R. Benefit, in *Function, Phylogeny, and Fossils*, D. R. Begun, C. V. Ward, M. D. Rose, Eds. (Plenum, New York, 1997), pp. 241–267.
7. D. R. Begun, C. V. Ward, M. D. Rose, in *Function, Phylogeny, and Fossils*, D. R. Begun, C. V. Ward, M. D. Rose, Eds. (Plenum, New York, 1997), pp. 389–415.
8. L. S. B. Leakey, *Ann. Mag. Nat. Hist.* **13**, 689 (1962).
9. M. Pickford, *J. Hum. Evol.* **14**, 113 (1985).
10. ———, *Z. Morph. Anthropol.* **76**, 117 (1986).
11. ———, in *Primate Evolution*, vol. 1, J. G. Else and P. C. Lee, Eds. (Cambridge Univ. Press, Cambridge, 1986), pp. 163–171.
12. P. Andrews, *Nature* **360**, 641 (1992).
13. T. Harrison, *Primates* **33**, 501 (1992).
14. D. R. Begun, *Yrbk. Phys. Anthropol.* **37**, 11 (1994).
15. C. B. Ruff, *J. Hum. Evol.* **17**, 687 (1988); K. L. Rafferty, A. Walker, C. B. Ruff, M. D. Rose, P. Andrews, *Am. J. Phys. Anthropol.* **97**, 391 (1995); G. Conroy, *Int. J. Primatol.* **8**, 115 (1987).
16. J. Kelley, *Am. J. Phys. Anthropol.* **96**, 365 (1995).
17. Preliminary descriptions of large hominoid specimens from Nachola (20, 23, 24) and differences in the morphology of hominoid humeri from Maboko (35) suggest that material herein assigned to *Equatorius* may comprise more than one species.
18. M. D. Rose, in *Function, Phylogeny, and Fossils*, D. R. Begun, C. V. Ward, M. D. Rose, Eds. (Plenum, New York, 1997), pp. 79–100.
19. C. V. Ward, in *Function, Phylogeny, and Fossils*, D. R. Begun, C. V. Ward, M. D. Rose, Eds. (Plenum, New York, 1997), pp. 101–130.
20. M. Nakatsukasa, A. Yamanaka, Y. Kunimatsu, D. Shimizu, H. Ishida, *J. Hum. Evol.* **34**, 657 (1998).
21. The entire type series of *G. darvini* from Devínska Nová Ves, Slovakia, consists of four isolated molar teeth, which limits comparisons with other taxa. However, the two lower molars in the series (including the type specimen) have prominent buccal cingulae, a primitive hominoid character that is rare in *E. africanus* (6).
22. M. L. McCrossin and B. R. Benefit, *Proc. Natl. Acad. Sci. U.S.A.* **90**, 1962 (1993).
23. M. D. Rose, *Afr. Std. Monogr. Suppl.* **24**, 3 (1996).
24. H. Ishida, M. Pickford, H. Nakaya, Y. Nakano, *ibid.* **2**, 73 (1984).
25. McCrossin and Benefit (6) propose that new upper central incisors from Maboko extend the range of variation from the site to encompass the morphology of the Fort Ternan incisor. However, details of these specimens have not yet been described, and we emphasize that the morphology of the several available incisors from Maboko, Majiwa, and Kipsaramon is remarkably uniform and discretely different from that of *K. wickeri* at Fort Ternan.
26. J. Kelley, *Am. J. Phys. Anthropol.* **96**, 390 (1995).
27. KNM-FT 28 has an index of relative canine height (crown height divided by maximum mesiodistal length) of 1.62. The value for the canine belonging to KNM-TH 28860 is 1.35. Ranges of values and sample sizes for *Proconsul* and *Afropithecus* are, respectively, 1.40 to 1.50 (9) and 1.14 to 1.18 (2); for *Dryopithecus* and *Lufengpithecus* values are 1.54 to 1.61 (3) and 1.56 to 1.85 (7).
28. P. Andrews and A. Walker, in *Human Origins: Louis*

- Leakey and the East African Evidence, G. L. Isaac and E. R. McCown, Eds. (W. A. Benjamin, Menlo Park, CA, 1976), pp. 279–304.
29. L. Martin and P. Andrews, in *Species, Species Concepts, and Primate Evolution*, W. H. Kimbel and L. Martin, Eds. (Plenum, New York, 1993), pp. 393–427.
30. P. Andrews, T. Harrison, E. Delson, R. L. Bernor, L. Martin, in *The Evolution of Western Eurasian Neogene Mammal Faunas*, R. L. Bernor, V. Fahlbusch, H.-W. Mittman, Eds. (Columbia Univ. Press, New York, 1996), pp. 168–206.
31. J. Kelley, unpublished data. Features by which the two species can be differentiated have been identified in all of the anterior teeth, all the premolar teeth except P₄, and the maxilla.
32. Two distinct lower canine morphologies are now recognized in the Paşalar sample. Canines belonging to the unnamed species are uniformly higher crowned in relation to length than those assigned to *G. alpani*.
33. B. Alpagut, P. Andrews, L. Martin, *J. Hum. Evol.* **19**, 397 (1990).
34. Andrews (12) proposed phyletic links between *Kenyapithecus* and all Turkish Middle Miocene taxa. We

would restrict this relationship to the second, unnamed species at Paşalar.

35. M. L. McCrossin, *Am. J. Phys. Anthropol. Suppl.* **24**, 164 (1997).
36. This research forms part of the work of the Baringo Paleontological Research Project (BPRP), in collaboration with the National Museums of Kenya. We thank the Office of the President of the Republic of Kenya for permission to carry out research in Kenya. BPRP has been supported by grants to A.H. from NSF (SBR-9208903), the Louise H. and David S. Ingalls Foundation, the Louise I. Brown Foundation, Clayton Stephenson, and Yale University. J.K. acknowledges support from NSF grant SBR-9408664 and thanks B. Alpagut who kindly gave permission to study the Paşalar hominoids. We thank E. Mbua and the staff of the National Museums of Kenya for their support; P. Andrews, T. Harrison, and D. Pilbeam for valuable insights regarding the relationships of *Kenyapithecus*; B. Kimeu, who discovered KNM-TH 28860; K. Cheboi for assistance in the field; and S. McBrearty, who suggested the generic name. L. Anderson, J. Kingston, and M. Tomasco prepared the figures.

29 June 1999; accepted 30 July 1999

Fossil Plants and Global Warming at the Triassic-Jurassic Boundary

J. C. McElwain,* D. J. Beerling, F. I. Woodward

The Triassic-Jurassic boundary marks a major faunal mass extinction, but records of accompanying environmental changes are limited. Paleobotanical evidence indicates a fourfold increase in atmospheric carbon dioxide concentration and suggests an associated 3° to 4°C “greenhouse” warming across the boundary. These environmental conditions are calculated to have raised leaf temperatures above a highly conserved lethal limit, perhaps contributing to the >95 percent species-level turnover of Triassic-Jurassic megafloora.

The end-Triassic mass extinction event [205.7 ± 4 million years ago (Ma)] was the third largest in the Phanerozoic, resulting in the loss of over 30% of marine genera (1) and 50% of tetrapod species (2), >95% turnover of megafloreal species (3, 4), and marked microfloral turnover in Europe (5) and North America (6). Many causal mechanisms have been suggested (7), but because of the paucity of Triassic-Jurassic (T-J) oceanic sediments suitable for geochemical analyses (7–9), the associated environmental conditions remain poorly characterized and the causal mechanism or mechanisms equivocal. Here we provide a temporally detailed investigation of the atmospheric CO₂ and climatic conditions associated with the T-J mass extinctions, from analyses of the ecophysiological characteristics of fossil megafloreas preserved in composite terrestrial T-J sections in Jameson Land, East Greenland (10), and Scania, southern Sweden (11).

Evidence from sedimentary facies (12),

Department of Animal and Plant Sciences, University of Sheffield, Sheffield, S10 2TN, UK.

*To whom correspondence should be addressed. E-mail: J.McElwain@sheffield.ac.uk

paleosols (13), sea-level change (14), and flood basalt volcanism (15) all indirectly suggest perturbation of the T-J global C cycle. Therefore, likely atmospheric CO₂ variations across the T-J boundary were determined from the stomatal density (SD, number of pores per unit area) and stomatal index (SI, proportion of pores expressed as a percentage of epidermal cells) of fossil leaf cuticles from 7 genera from 16 beds in Jameson Land and 11 genera from 13 beds in Scania. SD and SI are inversely related to the ambient CO₂ concentration during growth (16, 17) and can be used to reconstruct geological time series of atmospheric CO₂ (18, 19). The standardized SD and SI records for both localities were obtained and corrected for changes in species composition between individual beds to remove taxonomic bias (20) (Fig. 1).

High-resolution records of SD and SI from both sites showed reductions during the middle Rhaetian persisting into the Hettangian and then returning to preexcursion values (Fig. 1). The reductions are consistent with an increase in atmospheric CO₂ concentration across the T-J boundary, in agreement with inferences from geochemical analyses of fos-

REPORTS

sil soils (13). SD, but not SI, is sensitive to changes in precipitation; however, the presence of coals at both localities throughout the Rhaetian and Hettangian indicates stability in

the local precipitation regime (3), and so this explanation for the reduction in SD can be discounted. The very low SI of fossil leaves across the T-J boundary (~3 to 4) has only

previously been observed in Lower Devonian fossil axes (~2 to 3) (21) that developed in CO₂ concentrations of between 2400 and 3000 parts per million (ppm) (22).

Atmospheric CO₂ concentrations were calculated from stomatal ratios [a ratio of the SI of the nearest living morphological or ecological (or both) equivalent of the fossil divided by the SI of the fossil taxa] of T-J Ginkgoales and Cycadales (Table 1) (21, 23). These calculations indicated that CO₂ increased from 600 to 2100-2400 ppm across the T-J boundary (Table 1, Fig. 2)—a more conservative rise than calculated from two Early Jurassic paleosols (4800 ppm) (13). A fourfold increase in CO₂ could have raised mean global temperatures by 3° to 4°C (Fig. 2) (24). The most probable source of this CO₂ was extensive T-J basaltic volcanicity associated with the breakup of Pangea, which produced the Central Atlantic Magmatic Province (CAMP, 199 ± 2.4 Ma), covering an estimated 7 × 10⁶ km² (15). If volcanism was the sole source of the T-J CO₂ rise (25), the maximum volume of basalt required to have produced 1500 to 1800 ppm CO₂ would be 3.6 × 10⁵ km³ (26), which is well within that estimated by Marzoli *et al.* (15) (2 × 10⁶ km³).

For terrestrial vegetation from Greenland and Sweden (paleolatitude ~45°) growing in high CO₂ (900 to 1200 ppm) and a warm end-Triassic climate (summer temperatures of >30°C) (27), the additional climatic warming may have impaired leaf photosynthetic function, severely reducing carbon uptake. To test this hypothesis, we calculated leaf temperatures from energy-balance con-

Fig. 1. Mean detrended stomatal densities (SD) and indices (SI) calculated [(as in (20))] from the primary data (Table 1) for (A) Scania, southern Sweden, and (B) Jameson Land, East Greenland. "Mega," "Micro," and "Trans" denote megafloral and microflora zonation and the transition flora in Greenland, respectively. Arrows indicate direction of time. The T-J boundary is recorded in Greenland at 50 m (10), and these strata are correlated with the Scanian strata by the first occurrence of *Thaumatopteris* flora at the base of the transition zone in Greenland and the *Thaumatopteris-Lepidopteris* boundary in Scania. The scales from Greenland (depth of plant-bearing beds of the Cape Stewart formation from the Jameson horizon in the Neills Cliff formation) and Sweden (position of plant-bearing beds or localities from composite sections of the Höganäs and Höör Sandstone formations of Scania) are not directly comparable beyond stage level. The succession of the different beds or localities in (A) are taken from (3). 1, Bjuv α; 2, Bjuv 1; 3, Höganäs Lower; 4, Stabbarp Ton 10; 5, Skromberga; 6, Bjuv 2 and 3; 7, Hyllinge; 8, Bosarp; 9, Bjuv 4; 10, Skromberga Upper; 11, Stabbarp N.U.G.; 12, Stabbarp J. Mol; 13, Höganäs Upper; 14, Helsingborg; 15, Palsjö; 16, Munka Tågarp; 17, Rodalsberg; 18, Dompang; 19, Sofiero; and 20, Höör. Dating of the boundary is from (34).

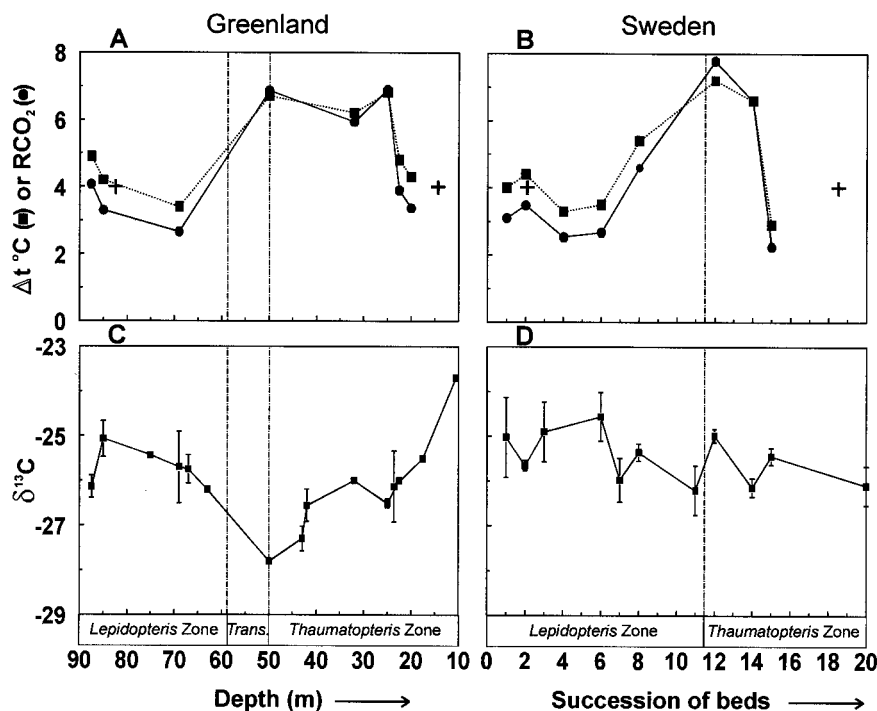
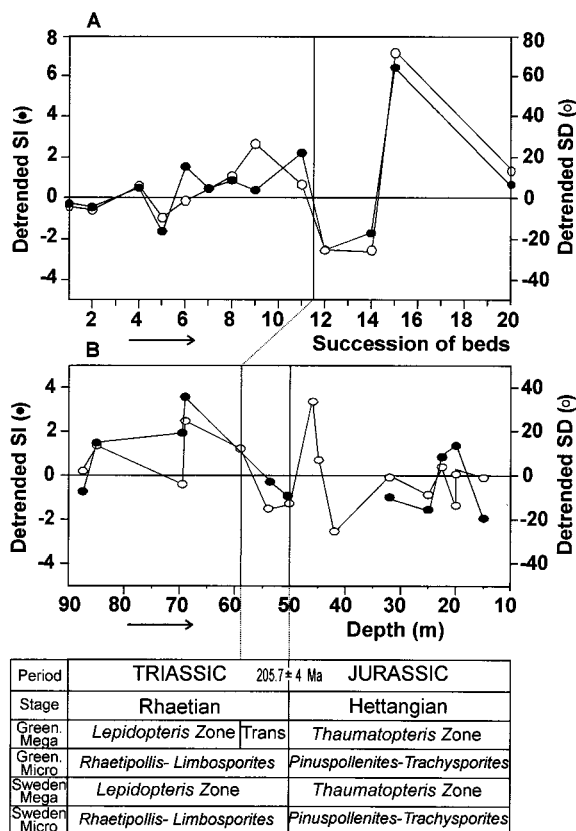


Fig. 2. Reconstructed atmospheric CO₂ concentration (ratio to present day) (solid line) calculated [as in (21)] from the stomatal ratios of a subset of species [Ginkgoalean and Cycadalean species only (Table 1)] from the total data set (as in Fig. 1) for (A) Greenland and (B) Sweden compared with model estimates (+) (22) and mean global temperature (Δt, in degrees Celsius) (dashed line) calculated from a CO₂-greenhouse formulation (24). RCO₂ is the ratio of reconstructed CO₂ concentration to a preindustrial value of 300 ppm. Mean stable carbon isotope composition (δ¹³C, in per mil) of fossil leaves from (C) Greenland and (D) Sweden used to constrain the leaf energy-balance model (Fig. 3) (28). The duration of CO₂ and temperature changes in (A) and (B) cannot be directly compared beyond stage level because of difference in scales. Arrows indicate direction of time.

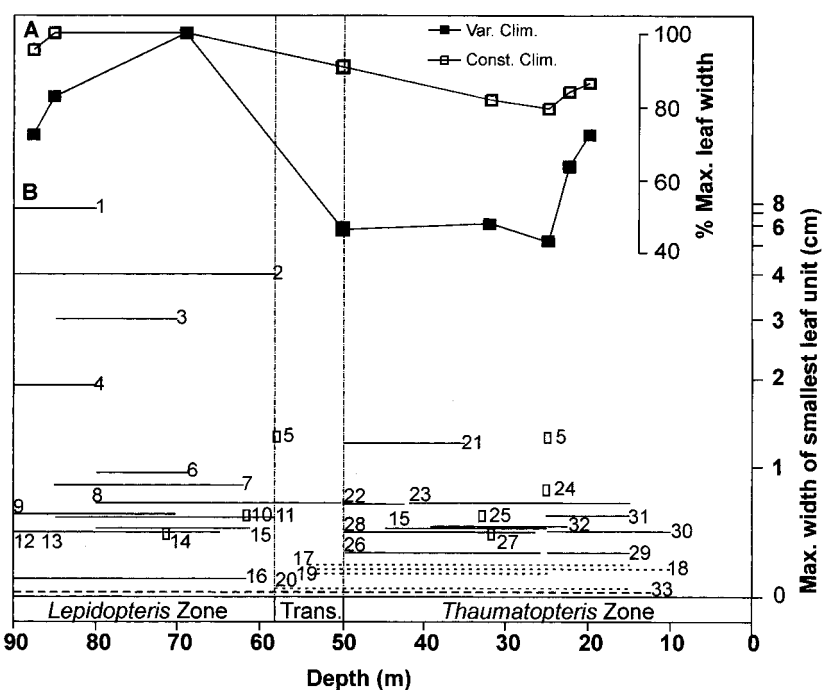
REPORTS

Table 1. Mean primary stomatal density (SD), index (SI), and ratio (SR) data in Jameson Land (per depth, 90 to 15 m) and in Scania (per bed or locality number, 1 to 20).

Bed (m)	Mean SD \pm SE (mm ⁻²)	Mean SI \pm SE	SD obs.*	S.I. obs.†	Fossil species used for SR analysis‡	SI \pm SE	SR
87.5	63.2 \pm 2.9	5.9 \pm 0.3	79(8)	79(8)	<i>Baeira boeggildiana</i>	6.4 \pm 0.6	2.04
85	78.2 \pm 5.2	6.8 \pm 0.7	7(1)	6(1)	<i>G. obovatus</i>	4.7 \pm 0.3	1.65
69.5	63.6 \pm 3.8	10.3 \pm 0.9	7(1)	7(1)	<i>G. obovatus</i>	6.8 \pm 0.7	1.65
69	89.6 \pm 13.8	9.1 \pm 0.9	18(3)	18(3)	<i>G. acosmica</i>	8.5 \pm 0.6	1.33
59	68.8 \pm 4.6		11(1)	n/a			
54	41.1 \pm 3.6	7.7 \pm 0.9	11(1)	11(1)			
50	46.1 \pm 2.6	6.2 \pm 0.4	47(3)	47(3)	<i>Stenopteris dinosaurensis</i>	3.3 \pm 0.3	3.43
46	91.1 \pm 5.3		7(1)	n/a			
42	38.8 \pm 3.2		11(1)	n/a			
32	21.8 \pm 2.1	3.8 \pm 0.4	9(1)	9(1)	<i>B. spectabilis</i>	3.8 \pm 0.4	2.97
25	13.2 \pm 1.1	3.3 \pm 0.3	15(1)	15(1)	<i>B. spectabilis</i>	3.3 \pm 0.3	3.45
22.5	25.3 \pm 2.3	5.8 \pm 0.5	16(1)	16(1)	<i>B. spectabilis</i>	5.8 \pm 0.5	1.95
20	42.4 \pm 3.3	9.2 \pm 0.7	7(1)	7(1)			
20	28.2 \pm 2.2	5.5 \pm 0.8	24(2)	24(2)			
20	39.7 \pm 2.4	5.3 \pm 0.7	27(2)	27(2)	<i>B. spectabilis</i>	6.7 \pm 0.8	1.69
15	50.5 \pm 9.6	4.9 \pm 0.8	6(1)	6(1)			
1	59.4 \pm 2.4	8.0 \pm 0.3	72(5)	72(5)	<i>Ctenis nilssonii</i>	6.5 \pm 0.4	1.55
2	39.9 \pm 1.7	7.0 \pm 0.3	79(5)	79(5)	<i>C. minuta</i> , <i>C. nilssonii</i>	5.8 \pm 0.6	1.75
4	83.1 \pm 3.4	9.2 \pm 0.3	109(8)	109(8)	<i>B. paucipartata</i>	8.9 \pm 1.1	1.27
5	53.6 \pm 5.9	8.9 \pm 0.9	15(5)	15(5)			
6	61.9 \pm 2.9	9.8 \pm 0.4	108(6)	108(6)	<i>B. minuta</i>	8.4 \pm 0.7	1.34
7	72.8 \pm 2.3	10.7 \pm 0.3	95(3)	95(3)			
8	65.7 \pm 1.8	7.9 \pm 0.2	291(6)	250(6)	<i>Baeira</i> sp.	4.9 \pm 0.3	2.31
9	107.9 \pm 4.6	9.9 \pm 1.1	9(1)	3(1)			
11	47.7 \pm 3.48	8.1 \pm 0.6	35(2)	35(2)			
12	28.5 \pm 2.94	3.8 \pm 0.3	59(2)	59(2)	<i>B. spectabilis</i>	2.9 \pm 0.2	3.89
14	19.1 \pm 2.0	3.9 \pm 0.4	12(1)	12(1)	<i>B. longifolia</i>	3.4 \pm 0.3	3.30
15	92.5 \pm 7.1	10.1 \pm 1.1	15(2)	15(2)	<i>Nilssonia polymorpha</i>	9.0 \pm 0.9	1.13
20	73.2 \pm 2.4	10.1 \pm 0.4	156(6)	156(6)			

*Total number of primary SD observations per bed or locality with number of species investigated in parentheses. †Total number of primary SI observations per bed or locality with number of species investigated in parentheses. ‡Mean primary SI data from the subset of Ginkgoalean and Cycadalean species used to calculate stomatal ratios (SR) (27), from which paleoatmospheric CO₂ estimates were made (Fig. 2).

Fig. 3. (A) Simulated changes in leaf width required to avoid thermal damage to the leaf photosynthetic system from a leaf-scale energy-balance-photosynthetic biochemistry model with (var. clim.) and without (const. clim.) the effects of the reconstructed CO₂ and temperature increases from Fig. 2 (28). **(B)** Observations of fossil leaf, leaflet, and dissection widths of 33 species from East Greenland (10). Species 1 to 16 (solid lines) are present only in the *Lepidopteris* and transition zones (Rhaetian), when CO₂ and temperature were rising (except 15). Species 17 to 20 (short-dashed lines) were established in the transition zone before the T-J boundary, when CO₂ and temperature were near maximum levels. Species 21 to 32 (solid lines) are present only in the *Thaumatopteris* zone (Hettangian), when CO₂ and temperature were elevated and then declining (Fig. 2). The leaf width of *Equisetites muensteri* (33, long-dashed line), one of the only species that occurs in all three floral zones, is notably smaller. 1, *Ginkgoites obovata*; 2, *Pterophyllum hanesianum*; 3, *Saginopteris serrata*; 4, *Otozamites* sp. A; 5, *Saginopteris halli*; 6, *Dictyophyllum exile*; 7, *P. schenki*; 8, *Anomozamites minor*; 9, *Todites scoresbyensis*; 10, *G. acosmii*; 11, *G. fimbriatus*; 12, *P. xiphopterum*; 13, *P. pinnatifidum*; 14, *Cladophlebis scariosa*; 15, *T. geoppertianus*; 16, *G. minuta*; 17, *T. princeps*; 18, *G. muensteriana*; 19, *Stenopteris dinosaurensis*; 20, *Czekanowskia nathorstii*; 21, *A. hartzi*; 22, *C. ingens*; 23, *T. recurvatus*; 24, *Osmundopsis plectrophora*; 25, *A. niteda*; 26, *D. nilssonii*; 27, *Gleicherites niteda*; 28, *A. marginatus*; 29, *G. taeniata*; 30, *G. hermelini*; 31, *C. svedbergi*; 32, *P. subaequale*; and 33, *Equisetites muensteri*.



siderations using measurements of fossil leaf width, stomatal density and size, and $\delta^{13}\text{C}$ (28). Two sets of calculations were performed, one with constant typical end-Triassic tropical climate (27) and CO_2 (22) and one with variable warming and variable CO_2 as reconstructed (Fig. 2). The results indicated that large leaves (>3 to 4 cm) in full sunlight of the upper canopy (that is, *Ginkgo*) or plants of open habitats could have reached noon temperatures at least 10°C above air temperatures, exceeding the observed heat limit for CO_2 uptake of present-day tropical taxa (29). Furthermore, transpirational cooling of leaves would have been much reduced at the T-J boundary because of very low stomatal densities (~25 to 40 mm^{-2}) reducing stomatal conductance, a feature exacerbated by the high leaf-to-air vapor pressure deficits occurring under high temperatures (30).

The extent of high-temperature injury to leaves across the T-J boundary would be size-dependent, because size influences boundary layer conductance and heat dissipation. Heat loss from leaves can be maximized by reductions in leaf size or increases in leaf dissection (or both) (29). Model simulations (28) indicate that the reconstructed rise in CO_2 and temperature (Fig. 2) would have caused size-dependent thermal damage to leaves, influencing the survival and distribution or extinction of large-leaved species at the T-J boundary. This hypothesis was tested by measuring the maximum width of the smallest leaf unit (that is, leaf, leaflet, or leaf dissection widths) in the Greenland flora, for which the sedimentary sequence is known to be more continuous than in Sweden (4). The only species common to both Upper Triassic and Lower Jurassic floral zones (seven species), in a flora of over 200 species, are characterized by highly dissected (*Clathropteris meniscoides* and *Todites geoppertiana*) or very narrow leaves (*Equisetites muensteri*) (Fig. 3). Furthermore, species of families most probably dominant in the upper canopy (such as Ginkgoales), with large entire leaves and the greatest predicted temperature overburden (such as *Ginkgoites obovatus*), appear to have been replaced by species with more dissected leaves (such as *G. fimbriatus*), over the initial period of increasing temperature and CO_2 , and extremely dissected leaves (*Czekanowskia* and *Baiera G. muensteriana*), under maximum temperature and CO_2 conditions (Figs. 2 and 3). A similar pattern of species extinction or replacement occurs within the *Anomozamites*, *Saginopteris*, *Todites*, *Dictyophyllum*, and *Pterophyllum*, the percentage reductions in leaf size of the replacement species being greatest among those taxa having greater initial leaf size (for example, reductions of 99, 80, and 60 to 10% were observed across the T-J boundary in genera with leaves or leaflets initially >5, 2 to 3, and 1 to 0.5 cm wide, respectively) (Fig. 3). All new species establishing in the transition zone (10)

had highly dissected or narrow leaves (0.1 to 1.5 cm wide) in all depositional environments (31).

The assumption of constant CO_2 and temperature across the boundary does not correlate with the observed reductions in leaf dimensions (Fig. 3). Furthermore, there is no evidence for aridity (as indicated by no increase in fossil plant $\delta^{13}\text{C}$ and the presence of coal) or marine incursion (as indicated by the absence of marine fossils) in Greenland, both of which could potentially drive selection for narrower or more dissected leaves. The fact that the observed reductions in leaf width parallel those predicted (Fig. 3) under an fourfold CO_2 rise and a 3° to 4°C warming of global climate independently corroborates these reconstructions. We therefore suggest that CAMP-induced "super greenhouse" conditions drove selection to avoid lethal leaf temperatures, resulting in extinctions and distributional changes that contributed to the observed >95% turnover of T-J megafloreal species in Europe (32).

References and Notes

1. D. M. Raup and J. J. Sepkoski, *Science* **215**, 1501 (1982); P. E. Olsen, N. H. Shubin, M. H. Anders, *ibid.* **237**, 1025 (1987).
2. E. H. Colbert, in *Dynamics of Extinction*, D. K. Elliot, Ed. (Wiley, New York, 1986), pp. 49–62; M. J. Benton, *Science* **268**, 52 (1995).
3. T. M. Harris, *Medd. Groen.* **112**, 1 (1937).
4. A. B. Lundblad, *K. Sven. Vetenskapsakad. Handl.* **6**, 1 (1959).
5. H. Visscher and W. A. Brugman, *Rev. Palaeobot. Palynol.* **34**, 115 (1981).
6. S. J. Fowell, B. Cornet, P. E. Olsen, *Spec. Pap. Geol. Soc. Am.* **288**, 197 (1994).
7. A. Hallam and P. B. Wignall, Eds., *Mass Extinctions and Their Aftermath* (Oxford Univ. Press, Oxford, UK, 1997).
8. R. Morante and A. Hallam, *Geology* **24**, 391 (1996).
9. C. A. McRoberts, H. Furrer, D. S. Jones, *Palaeogeogr. Palaeoclimatol. Palaeoecol.* **136**, 79 (1997).
10. The plant-bearing strata of the Cape Stewart formation, Jameson Land, are Rhaetian-Hettangian (3) in age, supported by palynological analysis [K. R. Pedersen and J. J. Lund, *Rev. Palaeobot. Palynol.* **31**, 1 (1980)]. These strata are marked by a >95% species-level turnover of megaflorea resulting in two distinct floral zones: a pre-T-J boundary (Rhaetian) flora characterized by the presence of *Lepidopteris* species and a post-T-J boundary (Hettangian) flora marked by the presence of *Thaumatopteris* species. A transition zone flora occurs over 6 m of the 90-m outcrop containing elements from both floral zones and is characterized by the first occurrence of *Thaumatopteris* zone species and the last occurrence of >95% of *Lepidopteris* zone species. The beds that mark the last occurrence of *Lepidopteris* zone species have been used to designate the T-J boundary beds in Greenland.
11. The plant-bearing strata of the Höganäs and Höör Sandstone formations, Scania, are Rhaetian-Hettangian in age (4), supported by palynological analysis [D. Guy-Ohlson, *Geol. Foeren. Foerh.* **103**, 233 (1981)] and the presence of generically comparable megaflorea to the *Lepidopteris* and *Thaumatopteris* zone flora of East Greenland (10). Transition zone flora [as in (10)] is absent in Scania.
12. A. Hallam, *Hist. Biol.* **10**, 247 (1995).
13. C. J. Yapp and H. Poeths, *Earth Planet. Sci. Lett.* **137**, 71 (1996).
14. A. Hallam, *J. Geol. Soc. London* **154**, 773 (1997).
15. A. Marzoli et al., *Science* **284**, 616 (1999).
16. F. I. Woodward, *Nature* **327**, 617 (1987).
17. _____ and F. A. Bazzaz, *J. Exp. Bot.* **39**, 1771 (1988).

18. D. J. Beerling and W. G. Chaloner, *Ann. Bot.* **71**, 431 (1992); D. J. Beerling, W. G. Chaloner, B. Huntley, J. A. Pearson, M. J. Tooley, *Proc. R. Soc. London. B Biol. Sci.* **251**, 133 (1993); J. Van der Burgh, J. Visscher, H. Dilcher, W. M. Kurschner, *Science* **260**, 1788 (1993); P. K. Van de Water, S. W. Leavitt, J. L. Betancourt, *ibid.* **264**, 239 (1994); J. C. McElwain, *Philos. Trans. R. Soc. London B* **353**, 83 (1998).
19. D. J. Beerling and F. I. Woodward, *Bot. J. Linn. Soc.* **124**, 137 (1997).
20. Primary SD and SI data (Table 1) were normalized according to $\bar{x} - x$, where \bar{x} is the genus mean for all beds or localities in either Greenland or Sweden and x is the genus mean per bed or locality. Normalized data were then corrected for any shifts in floral composition between individual beds by multiplying by the percentage composition of that genus at each of the beds or localities in Sweden and Greenland. These procedures were repeated for all individual genera to calculate an artificially genus-weighted trend. Mean genus-weighted SD and SI trends were calculated for both sites and removed from the normalized data to provide detrended stomatal records, which were independent of any floral composition changes between individual beds or localities.
21. J. C. McElwain and W. G. Chaloner [*Ann. Bot.* **76**, 389 (1995)] standardized the stomatal ratios (SR) of Upper Carboniferous fossil conifers against CO_2 estimates based on a long-term C cycle model (22) dictating a scale of $1\text{SR} = 2\text{RCO}_2 = 600 \text{ ppm } \text{CO}_2$, where RCO_2 is the ratio of atmospheric CO_2 concentration estimated from stomatal ratios relative to a preindustrial value of 300 ppm. *Ginkgo biloba* ($\text{SI} = 11.33 \pm 0.23$) and *Zamia furfuracea* ($\text{SI} = 10.12 \pm 0.27$) were assigned as the nearest living equivalent of the subset of fossil species chosen to calculate SRs (Table 1) and from these estimates of T-J CO_2 (Fig. 2).
22. R. A. Berner, *Science* **276**, 544 (1997).
23. J. C. McElwain and W. G. Chaloner, *Palaeos* **11**, 376 (1996).
24. The extent of associated climate change was calculated by assuming a greenhouse-gas relation between CO_2 and temperature with the use of a CO_2 -greenhouse formulation from Z. Kothavala, R. J. Oglesby, and B. Saltzman [*Geophys. Res. Lett.* **26**, 209 (1999)]:

$$\Delta T = 4.0 \ln(\text{RCO}_2)$$
 where ΔT is the difference in mean global surface air temperature. The estimates will be somewhat dependent on the responses of the thermohaline circulation [E. Barrera et al., *Geology* **25**, 715 (1997)].
25. The loss of marine primary productivity as a consequence of the end-Triassic extinctions may have contributed further to CO_2 accumulation in the atmosphere. A total shutdown of the oceanic biological pump can result in doubling of the ambient atmospheric CO_2 [J. L. Sarmiento and J. R. Toggweiler, *Nature* **308**, 621 (1984)]. Isotopic evidence supports a reduction in oceanic productivity at the T-J boundary (8); however, the data are equivocal because of potential diagenetic effects (8, 9).
26. According to K. Caldeira and M. R. Rampino [*Geophys. Res. Lett.* **18**, 987 (1991)], 1 to 2×10^{10} kg of CO_2 are released during the production of 1 km^3 of basalt.
27. K. M. Wilson et al., *Spec. Pap. Geol. Soc. Am.* **288**, 91 (1994).
28. The models of D. J. Beerling and W. P. Quick [*Global Change Biol.* **1**, 289 (1995)] and D. J. Beerling and F. I. Woodward (19) were used to estimate T-J leaf temperatures with the use of fossil stomatal characteristics to define maximal stomatal conductance, whereas the responses of stomatal conductance to CO_2 , water vapor pressure deficit of the air, and irradiance were based on the responses of extant species. Simulated photosynthetic and stomatal conductance responses to typical uniform diurnal tropical climatic conditions [mean temperatures determined from (27), relative humidity (60%), and wind speed (1 m s^{-1})] were constrained so that the predicted leaf $\delta^{13}\text{C}$ (33) equals the fossil observation of leaf $\delta^{13}\text{C}$ (Fig. 2). These simulated leaf characteristics were then used to determine the maximum leaf size that can just avoid lethal temperatures (48°C) (29) when daily maximum irradiance (2000 $\mu\text{mol m}^{-2} \text{ s}^{-1}$) and close to daily maximum temperatures are

- reached. This approach was used to estimate relative maximum leaf size during the period of study (Fig. 3).
29. The threshold for thermal damage of nonsucculent leaves (45° to 52°C) is a highly conserved characteristic across a wide range of extant taxa [W. Larcher, in *Ecophysiology of Photosynthesis*, E. D. Schultze and M. M. Caldwell, Eds. (Springer-Verlag, Berlin, 1994), pp. 261–277; Y. Gauslaa, *Holarct. Ecol.* **7**, 1 (1984)], implying little evolutionary change through time.
 30. T. A. Mansfield, A. M. Hetherington, C. J. Atkinson, *Annu. Rev. Plant Physiol. Plant Mol. Biol.* **41**, 55 (1990).
 31. A review of fossil Ginkgoalean leaves revealed that species with the most dissected leaves, characterized by multidichotomies 0.5 to 2 mm wide, are restricted to Late Triassic to early Middle Jurassic facies [T. Kimura, G. Naito, T. Ohana, *Bull. Natl. Sci. Mus. Tokyo* **9**, 91 (1983)].
 32. The cause of T-J floral turnover has traditionally been attributed to a sedimentary hiatus (3). However, this hypothesis is unsupported by sedimentological evidence [G. Dam and F. Surlyk, *Geology* **20**, 749 (1992); *Spec. Publ. Int. Assoc. Sedimentol.* **18**, 4189 (1993)], which identifies no major facies changes or unconformities between the T-J strata in Greenland. Furthermore, the absence of the upper Rhaetian *Ricciisporites-Polypodisporites* acme zone [W. M. L. Schuurman, *Rev. Palaeobot. Palynol.* **23**, 159 (1977)] in Greenland (10) and Sweden (11), which has also been tentatively interpreted as evidence of a hiatus at both localities, is questionable, as acme zones are generally considered of only local use, owing to the effects of ecological, environmental, and postdepositional processes on relative pollen abundances.
 33. The value of $\delta^{13}\text{C}$ is

$$\delta^{13}\text{C} = \left\{ \left[\frac{^{13}\text{C}_{\text{unk}}/^{12}\text{C}_{\text{unk}}}{^{13}\text{C}_{\text{std}}/^{12}\text{C}_{\text{std}}} \right] - 1 \right\} \times 1000$$
 where unk the ratio of unknown to sample and std is the ratio of the pee dee belemnite standard.
 34. F. M. Grandstein *et al.*, *J. Geophys. Res.* **99**, 24051 (1994).
 35. We thank E. M. Friis (Swedish Museum of Natural History) and S. Funder (Danish Geological Museum) for loans and provision of fossil leaves; P. E. Olsen, F. Surlyk, W. G. Chaloner, D. J. Read, R. A. Spicer, C. K. Kelly, and P. Wignall for comments on earlier versions; and the Isotope Laboratory at Royal Holloway College, University of London, for making measurements of $\delta^{13}\text{C}$. We gratefully acknowledge funding from the Natural Environment Research Council, UK (GR9/02930), and through Royal Society Research Fellow and Equipment grants to D.J.B.

21 April 1999; accepted 26 July 1999

Gene Expression Profile of Aging and Its Retardation by Caloric Restriction

Cheol-Koo Lee,^{1,3} Roger G. Klopp,²
Richard Weindruch,^{4*} Tomas A. Prolla^{3*}

The gene expression profile of the aging process was analyzed in skeletal muscle of mice. Use of high-density oligonucleotide arrays representing 6347 genes revealed that aging resulted in a differential gene expression pattern indicative of a marked stress response and lower expression of metabolic and biosynthetic genes. Most alterations were either completely or partially prevented by caloric restriction, the only intervention known to retard aging in mammals. Transcriptional patterns of calorie-restricted animals suggest that caloric restriction retards the aging process by causing a metabolic shift toward increased protein turnover and decreased macromolecular damage.

Most multicellular organisms exhibit a progressive and irreversible physiological decline that characterizes senescence, the molecular basis of which remains unknown. Postulated mechanisms include cumulative damage to DNA leading to genomic instability, epigenetic alterations that lead to altered gene expression patterns, telomere shortening in replicative cells, oxidative damage to critical macromolecules by reactive oxygen species (ROS), and nonenzymatic glycation of long-lived proteins (1, 2).

Genetic manipulation of the aging process in multicellular organisms has been achieved in *Drosophila* through the overexpression of

catalase and Cu/Zn superoxide dismutase (3), in the nematode *Caenorhabditis elegans* through alterations in the insulin receptor signaling pathway (4), and through the selection of stress-resistant mutants in either organism (5). In mammals, mutations in the Werner Syndrome locus (WRN) accelerate the onset of a subset of aging-related pathology in humans (6), but the only intervention that appears to slow the intrinsic rate of aging is caloric restriction (CR) (7). Most studies have involved laboratory rodents which, when subjected to a long-term, 25 to 50% reduction in calorie intake without essential nutrient deficiency, display delayed onset of age-associated pathological and physiological changes and extension of maximum lifespan. Postulated mechanisms of action include increased DNA repair capacity, altered gene expression, depressed metabolic rate, and reduced oxidative stress (7).

To examine the molecular events associated with aging in mammals, we used oligonucleotide-based arrays to define the transcriptional response to the aging process in mouse gastrocnemius muscle. Our choice of tissue was guided by the fact that skeletal muscle is primarily composed of long-lived, high oxygen-consuming postmitotic cells, a

feature shared with other critical aging targets such as heart and brain. Loss of muscle mass (sarcopenia) and associated motor dysfunction is a leading cause of frailty and disability in the elderly (8). At the histological level, aging of gastrocnemius muscle in mice is characterized by muscle cell atrophy, variations in size of muscle fibers, presence of lipofuscin deposits, collagen deposition, and mitochondrial abnormalities (9).

A comparison of gastrocnemius muscle from 5-month (adult) and 30-month (old) mice (10–12) revealed that aging is associated with alterations in mRNA levels, which may reflect changes in gene expression, mRNA stability, or both. Of the 6347 genes surveyed in the oligonucleotide microarray, only 58 (0.9%) displayed a greater than twofold increase in expression levels as a function of age, whereas 55 (0.9%) displayed a greater than twofold decrease in expression. These findings are in agreement with a differential display analysis of gene expression in tissues of aging mice (13). Thus, the aging process is unlikely to be due to large, widespread alterations in gene expression.

Functional classes were assigned to genes displaying the largest alterations in expression (Table 1). Of the 58 genes that increased in expression with age, 16% were mediators of stress responses, including the heat shock factors Hsp71 and Hsp27, protease Do, and the DNA damage-inducible gene GADD45 (14). The largest differential expression between adult and aged animals (a 3.8-fold induction) was observed for the gene encoding the mitochondrial sarcomeric creatine kinase, a critical target for ROS-induced inactivation (15).

A consequence of skeletal muscle aging is loss of motor neurons followed by reinnervation of muscle fibers by the remaining intact neuronal units (16). Genes involved in neuronal growth accounted for 9% of genes highly induced in 30-month-old animals, including neurotrophin-3 (17), a growth factor induced during reinnervation, and synaptic vesicle protein-2, implicated in neurite extension (18). PEA3, a transcriptional factor induced in the response to

¹Environmental Toxicology Center, ²Institute on Aging, ³Departments of Genetics and Medical Genetics, University of Wisconsin, Madison, WI 53706, USA. ⁴Department of Medicine and Wisconsin Regional Primate Research Center, University of Wisconsin, Madison, WI and Veterans Administration Hospital, Geriatric Research, Education and Clinical Center, Madison, WI 53705, USA.

*To whom correspondence should be addressed at Department of Medicine, VA Hospital (GRECC 4D), 2500 Overlook Terrace, Madison, WI 53705, USA. E-mail: rhweindr@facstaff.wisc.edu (R.W.); Departments of Genetics and Medical Genetics, 445 Henry Mall, University of Wisconsin, Madison, WI 53706, USA. E-mail: taprolla@facstaff.wisc.edu (T.A.P.)